



PERGAMON

Pattern Recognition 34 (2001) 1459–1467

PATTERN  
RECOGNITION

THE JOURNAL OF THE PATTERN RECOGNITION SOCIETY

www.elsevier.com/locate/patcog

# Morphological surface profile extraction with multiple range sensors

Billur Barshan\*, Deniz Başkent<sup>1</sup>

*Department of Electrical Engineering, Bilkent University, Bilkent, 06533 Ankara, Turkey*

Received 24 September 1999; received in revised form 24 May 2000; accepted 24 May 2000

## Abstract

A novel method is described for surface profile extraction based on morphological processing of multiple range sensor data. The approach taken is extremely flexible and robust, in addition to being simple and straightforward. It can deal with arbitrary numbers and configurations of sensors as well as synthetic arrays. The method has the intrinsic ability to suppress spurious readings, crosstalk, and higher-order reflections, and process multiple reflections informatively. The performance of the method is investigated by analyzing its dependence on surface structure and distance, sensor beamwidth, and noise on the time-of-flight measurements. © 2001 Pattern Recognition Society. Published by Elsevier Science Ltd. All rights reserved.

*Keywords:* Morphological processing; Range sensing; Feature extraction; Surface profile extraction; Map building; Pattern analysis

## 1. Introduction

An inexpensive, yet effective and reliable approach to machine perception is to employ multiple simple range sensors coupled with appropriate data processing. The approach described here is aimed at the determination of arbitrary surface profiles, and is completely novel in that morphological processing techniques are applied to range data in the form of an arc map, representing angular uncertainties. The method is extremely flexible and can easily handle arbitrary sensor configurations as well as synthetic arrays obtained by moving a relatively small number of sensors. In contrast, approaches based on geometrical or analytical modeling are often limited to elementary target types or simple sensor configurations [1,2]. A commonly noted disadvantage of range sensors is the difficulty associated with interpreting spuri-

ous readings, crosstalk, higher-order and multiple reflections. The proposed method is capable of effectively suppressing the first three of these, and has the intrinsic ability to process echoes returning from surface features further away than the nearest (i.e., multiple reflections) informatively.

The essential idea of this paper — the use of multiple range sensors combined with morphological processing — can be applied to different physical modalities of range sensing of vastly different scales and in many different areas. These may include radar, sonar, optical sensing and metrology, remote sensing, ocean surface exploration, geophysical exploration, robotics, and acoustic microscopy.

Despite the generality of the method, for concreteness, we consider simple range sensors that measure time-of-flight (TOF)  $t_0$ , which is the round-trip travel time of the pulse between the sensor and the object. Given the speed of transmission  $c$ , the range  $r$  can be easily calculated from  $r = ct_0/2$ . Although such devices return accurate range data, typically they cannot provide direct information on the angular position of the object from which the reflection was obtained. Thus, all that is known is that the reflection point lies on a circular arc of radius  $r$ , as illustrated in Fig. 1(a). More generally, when one sensor

\* Corresponding author. Tel.: + 90-312-290-2161; fax: + 90-312-266-4192.

E-mail address: billur@ee.bilkent.edu.tr (B. Barshan).

<sup>1</sup> Current address: Department of Biomedical Engineering, University of Southern California, Los Angeles, CA 90089-1451, USA.

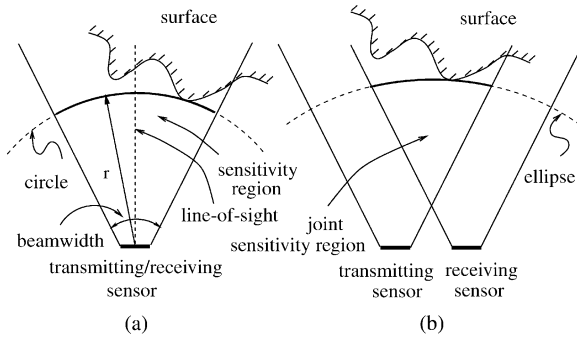


Fig. 1. (a) For the same sensor transmitting and receiving, the reflecting point is known to be on the circular arc shown. (b) The elliptical arc if the wave is transmitted and received by different sensors.

transmits and another receives, it is known that the reflection point lies on the arc of an ellipse whose focal points are the transmitting and receiving elements [Fig. 1(b)]. The arcs are tangential to the reflecting surface at the actual point(s) of reflection.

Most commonly, the wide beamwidth of the sensor is accepted as a device limitation that determines the angular resolving power of the system, and the reflection point is assumed to be along the line-of-sight. In our method, circular or elliptical arcs, representing the uncertainty of the object location, are drawn. By combining the information inherent in a large number of such arcs, angular resolution far better than that implied by the beamwidth is obtained.

## 2. Morphological surface profile extraction

Structured sensor configurations such as linear and circular arrays as well as irregularly configured sensors have been considered in Ref. [3], where the method of this paper is also generalized to moving sensors and synthetic arrays.

### 2.1. A motivating example

As an illustrative example of the method, Fig. 2(a) shows a surface whose profile is to be determined by using an irregular sensor configuration. A considerably large number of arcs can be obtained with a reasonable number of sensors because each sensor can receive pulses transmitted from all the others, provided a reflection point lies in the joint sensitivity region of that sensor pair. For sensors with large beamwidth, the number of arcs drawn approaches the square of the number of sensors. Fig. 2(b) shows the arcs obtained. Although each arc represents considerable uncertainty as to the angular position of the reflection point, one can almost extract

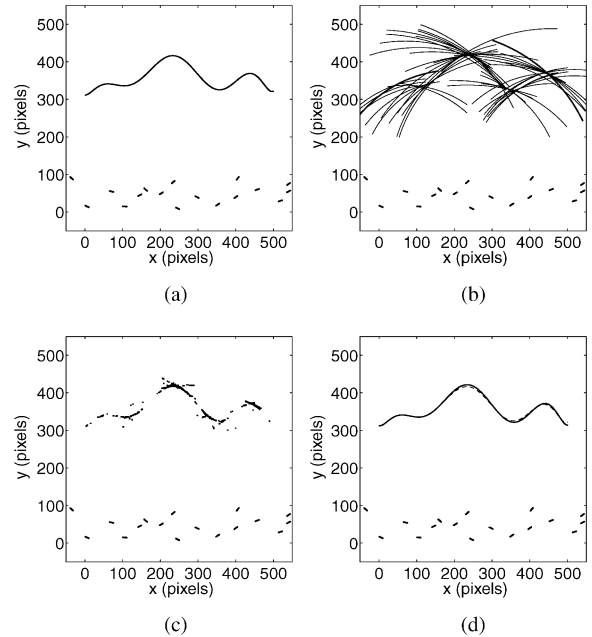


Fig. 2. (a) The actual surface and the sensor configuration, (b) the arc map obtained with an array of 17 sensors, each of  $45^\circ$  beamwidth, (c) the result of  $n = 6$  thinning, (d) the fitted curve (solid line) and the original surface (dashed line).  $E_1 = 2.75$  pixels,  $E_2 = 0.10$ .

the actual curve shown in Fig. 2(a) by visually examining the arc map in Fig. 2(b). Each arc drawn is expected to be tangential to the surface at least at one point. At these actual reflection point(s), several arcs will intersect with small angles at nearby points on the surface. The many small segments of the arcs superimposed in this manner coincide with and cover the actual surface, creating the darker features in Fig. 2(b) that reveal the surface profile. The remaining parts of the arcs, not actually corresponding to any reflections and simply representing the angular uncertainty of the sensors, remain more sparse and isolated. Similarly, those arcs caused by higher-order reflections, crosstalk, and noise also remain sparse and lack reinforcement.

### 2.2. Mathematical morphology

In this study, morphological operators are used to eliminate the sparse and isolated segments, spikes or extrusions in the arc map, leaving behind the mutually reinforcing segments that directly reveal the original surface profile. Erosion, dilation, opening, closing, and thinning are widely used morphological operations to accomplish tasks such as edge detection, skeletonization, segmentation, texture analysis, enhancement, and noise removal in image processing [4]. Mathematical morphology has been applied in diverse areas such as pattern and

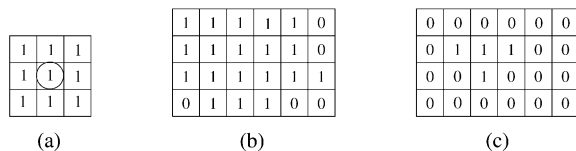


Fig. 3. An example for erosion: (a) the template, (b) the original image, and (c) the image after erosion.

shape analysis [5], machine vision [6], medical imaging [7], remote sensing [8], automatic target recognition [9], flaw detection [10], and atomic force microscopy [11]. Although most applications involve processing of conventional binary or gray-scale images, in some cases, range images are processed where the range information is coded in the gray-levels of the image [12,13]. The present approach is completely novel in that morphological processing is applied to range data in the form of an arc map, representing angular uncertainties.

Morphological operations basically consist of a set of simple rules to modify images: *Erosion* and *dilation* are the two fundamental morphological operations used to thin and fatten an image respectively. These operations are defined according to a structuring element or template. In this study, the structuring element for dilation and erosion is chosen to be the  $3 \times 3$  square template, shown in Fig. 3(a) with the central pixel circled.

A simple algorithm for erosion is as follows: The template is shifted over the pixels of the arc map image which take the value 1 one at a time and the template's pixels are compared with those pixels which overlap with the template [14]. For the  $3 \times 3$  square template used in this study, if all eight neighbors of a pixel with value one equal one, that pixel preserves its value, otherwise its value is set equal to zero. This way, the image will be eroded or shrunk in all directions by one pixel. An example to erosion is presented in Figs. 3(b) and (c). On the other hand, the dilation operation is used to fatten an image according to the template. This time, all eight neighbors of those image pixels which originally equal 1 are set equal to 1.

*Thinning* is a generalization of erosion with a parameter  $n$  varying in the range  $1 \leq n \leq 8$ . In this case, it is sufficient for any  $n$  neighbors of an image pixel to equal 1 in order for that pixel to preserve its value of one. The flexibility that comes with this parameter enables one to make more efficient use of the information contained in the arc map.

In *pruning*, which is a special case of thinning, at least one ( $n = 1$ ) of the neighboring pixels must have the value 1 in order for the central pixel to remain equal to 1 after the operation. This operation is used to eliminate isolated points [4]. Thus, pruning and erosion are the two extremes of thinning with  $n = 1$  and 8, respectively.

In some cases, the direct use of erosion may eliminate too many points and result in the loss of information

characterizing the surface. For such cases, the compound operations of *opening* and *closing* are considered. Opening consists of erosion followed by dilation, and vice versa for closing. Opening helps reduce small extrusions, whereas closing enables one to fill the small holes inside the image [15]. Closing is applied prior to thinning in cases where the points are not closely connected to each other so that the direct use of thinning may result in the loss of too many points. Filling the gaps using closing first may prevent excessive point loss from occurring.

The arc map itself and therefore the result after morphological processing naturally depend on the sensor configuration, image resolution, as well as surface and sensor parameters discussed in Section 3.

### 2.3. Curve fitting and error measures

The result of applying  $n = 6$  thinning to the arc map shown in Fig. 2(b) is presented in Fig. 2(c). As a last step, a least-squares polynomial fit is obtained to represent the surface profile compactly. The curve fitted to the thinned map in Fig. 2(c) is displayed in Fig. 2(d). In all of the examples in this paper, polynomials are of order 10. Although polynomial fitting has been found to be satisfactory in all of the cases considered, other curve representation approaches such as the use of splines might be considered as alternatives to polynomial fitting. Two error measures, both comparing the final polynomial fit with the actual curve, are employed:

$$E_1 = \sqrt{\frac{1}{N} \sum_{i=1}^N [p(x_i) - y(x_i)]^2}, \quad (1)$$

$$E_2 = \frac{E_1}{\sigma_y}. \quad (2)$$

The first is a root-mean-square absolute error measure, whereas the second is a dimensionless relative error measure with respect to the variation of the actual curve.  $N$  is the total number of columns in the map matrix,  $p(x_i)$  are the samples of the fitted polynomial, and  $\sigma_y^2 = (1/N) \sum_{i=1}^N [y(x_i) - (1/N) \sum_i y(x_i)]^2$  is the variance of the actual surface profile  $y(x_i)$ . In the simulations, where the actual surface is known, it is possible to choose the optimal value of the thinning parameter  $n$  minimizing  $E_1$  or  $E_2$ . In real practice, this is not possible so that one must use a value of  $n$  judged appropriate for the class of surfaces under investigation.

### 2.4. Sample experiments

We now consider the experimentally obtained arc map shown in Fig. 4(a). This data were collected with a real sonar ranging system, from a cardboard surface constructed in our laboratory. An array of five sonar sensors has been moved horizontally over a distance of 1.5 m to

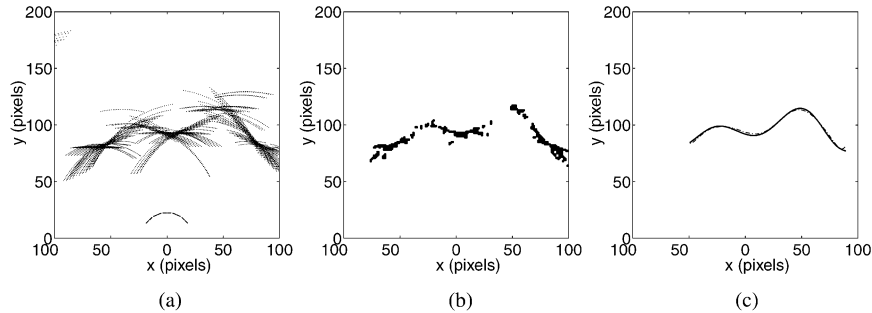


Fig. 4. (a) The sonar arc map and the sensor configuration. The data are collected from the surface at every 2.5 cm by translating the array from  $(-75, 0)$  to  $(75, 0)$ . (b) Result of erosion ( $n = 8$ ) followed by pruning ( $n = 1$ ). (c) The fitted curve (solid line) and the original surface (dashed line) resulting in  $E_1 = 1.11$  pixels and  $E_2 = 0.13$ .

increase the total number of arcs, collecting data every 2.5 cm. In the resulting arc map, there are some arcs which are not tangent to the actual surface at any point [e.g., the isolated arcs in the upper-left part of Fig. 4(a)]. These correspond to spurious data due to higher-order reflections, readings from other objects in the environment, or totally erroneous readings. These points are readily eliminated by the morphological processing [Fig. 4(b)]. The polynomial fit shown in Fig. 4(c) is a quite accurate representation of the original surface, with  $E_1 = 1.11$  pixels and  $E_2 = 0.13$ .

Next, we consider the arc map shown in Fig. 5(a), obtained from an array of three sonar sensors mounted on a mobile robot following the walls of a rectangular room [16]. The room is comprised of smooth planar walls, corners, an edge, and a corner entranceway. In Fig. 5(b), the result of morphological processing is shown. The spurious arc segments caused by the higher-order reflections have been eliminated. The method is most strained when features with large curvature (e.g., corners and edges of the room) are encountered in the environment since the method exploits neighboring relationships and local continuity (i.e., smoothness). The net effect is that the vertices of the sharp corners and edges are rounded (i.e., low-pass filtered). This corresponds to the spatial frequency resolving power of the system as determined by the chosen grid spacing.

Even though the method was initially developed and demonstrated for specularly reflecting surfaces, subsequent tests with Lambertian surfaces of varying roughness have indicated that the method also works for rough surfaces, with errors slightly increasing with roughness [17].

Structured arrays are often preferred in theoretical work for simplicity and ease of analysis, whereas the method presented here can handle irregular arrays equally easily. Although the problem of optimal sensor placement is a subject for future research, the large number of simulations performed indicate that it is preferable to work with irregular arrays, since the randomized van-

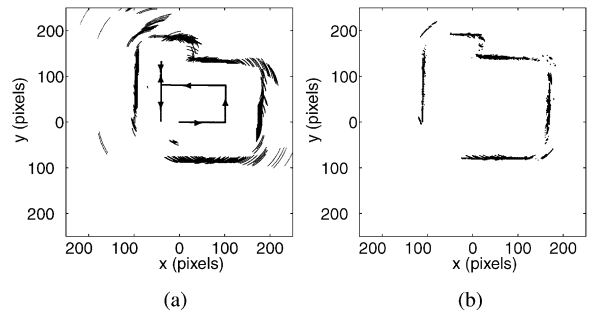


Fig. 5. (a) Sonar arc map and the path followed by the robot. (b) The result of  $n = 4$  thinning.

tage points of the sensors tend to complement each other better than structured ones. A detailed study of the effect of using different sensor configurations and morphological operations can be found in Ref. [3].

### 3. Performance of the method

Although the method is applicable to arbitrary surfaces, for the purpose of investigating the performance and the limitations of the method, from now on, we concentrate on sinusoidal surfaces whose parameters can be systematically varied. Simulations have been undertaken on sinusoidal surfaces of varying amplitude and periodicity, located at varying distances from the sensor array. These parameters are illustrated in Fig. 6(a).  $A$  is the peak-to-peak amplitude and  $T$  is the period of the sinusoidal surface,  $L$  is the vertical distance of the surface measured from  $y = 0$ . The elements of the sensor array are distributed in the box  $[-35, 440] \times [0, 90]$ , and the average vertical distance of the sensors from  $y = 0$  is 32.7 pixels.

We investigate the dependence of the error measures  $E_1$  and  $E_2$  on amplitude, period, surface distance, and sensor beamwidth. Additionally, the noise tolerance of the method is studied by introducing zero-mean additive

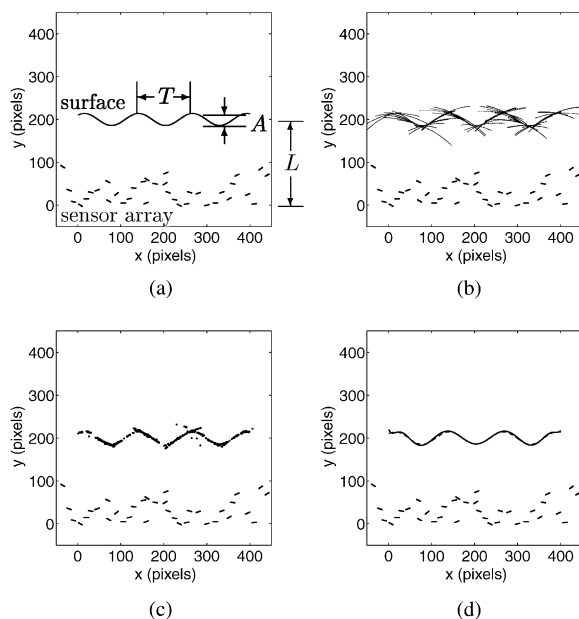


Fig. 6. (a) The actual surface and the definition of the parameters  $A$ ,  $T$ , and  $L$ , (b) the arc map obtained with an array of 35 sensors, each of  $30^\circ$  beamwidth, (c) the result of  $n = 3$  thinning, (d) the fitted curve (solid line) and the original surface (dashed line).  $E_1 = 2.03$  pixels,  $E_2 = 0.20$ .

white noise to the TOF readings. For this purpose, the sinusoid shown in Fig. 6(a), with  $A = 30$ ,  $T = 125$ , and  $L = 200$  pixels, is taken as a reference. The parameters  $A$ ,  $T$ , and  $L$  are varied around these values. The arc map generated for the sinusoid shown in Fig. 6(a) is shown in Fig. 6(b). The result of  $n = 3$  thinning, which gives the minimum errors for this example, is given in Fig. 6(c). The resulting errors when various morphological operators are applied to the same arc map are summarized in Table 1. Finally, the result of curve fitting, and the comparison with the actual surface are given in Fig. 6(d).

Table 1  
Results of various morphological operations

Morphological operation	$E_1$ (pixels)	$E_2$
Thinning ( $n = 1$ : pruning)	2.41	0.24
Thinning ( $n = 2$ )	2.21	0.22
Thinning ( $n = 3$ )	2.03	0.20
Thinning ( $n = 4$ )	2.09	0.21
Thinning ( $n = 5$ )	2.46	0.24
Closing and pruning ( $n = 1$ )	2.61	0.26
Closing and thinning ( $n = 3$ )	3.02	0.30
Closing and erosion ( $n = 8$ )	3.63	0.36

### 3.1. The effect of varying the period

First, the period is varied by keeping the amplitude and the surface distance constant at  $A = 30$  pixels and  $L = 200$  pixels, respectively.  $E_1$  and  $E_2$  both increase with decreasing period as expected [Figs. 7(a) and (b)]. For periods shorter than 100 pixels, the error increases significantly. The minimum radius of curvature  $R_{\min}$  is a useful indicator of the difficulty of extracting the profile: features with smaller radii of curvature are more difficult to accurately determine. For this reason, the relation between the minimum radius of curvature and period of the sinusoid is also plotted in Fig. 7(c).

### 3.2. The effect of varying the amplitude

In the next step, the amplitude is varied while keeping the period and the distance constant at  $T = 125$  pixels and  $L = 200$  pixels.  $E_1$  and  $E_2$  increase with increasing amplitude since this reduces the minimum radius of curvature, as shown in Fig. 8. However,  $E_2$  does not grow as fast as  $E_1$  since it is a measure of the error relative to  $\sigma_y$  which increases linearly with amplitude. Again, the minimum radius of curvature is plotted as a function of the amplitude in Fig. 8(c).

To get a better understanding of the relation between these errors and curvature, the results in Figs. 7 and 8 are rearranged to plot  $E_1$  versus minimum radius of curvature  $R_{\min}$  (Fig. 9). As expected, decreasing the curvature (hence increasing  $R_{\min}$ ) results in lower  $E_1$ . The fact that the solid and dashed lines (which represent varying  $T$  and  $A$ , respectively) follow each other closely, suggests that what really matters is not the individual values of  $T$  and  $A$ , but the value of  $R_{\min}$ .

### 3.3. The effect of varying the surface distance

Next, the distance to the surface is varied around  $L = 200$  pixels while the amplitude and the period are kept constant at  $A = 30$  pixels and  $T = 125$  pixels. As shown in Figs. 10(a) and (b), both  $E_1$  and  $E_2$  increase as the surface distance increases beyond  $L = 250$  pixels. Because the surface shape does not change, the curvature remains constant. (In this example,  $R_{\min} = 28.3$  pixels.) Details about the processing involved to generate Fig. 10 are presented in Table 2. Since the number of arc points obtained strongly depends on  $L$ , and since the most suitable morphological operation depends strongly on the density of arc points, the morphological procedure best suited to each value of  $L$  has been employed in constructing Fig. 10. In other words, the morphological rule has been customized for each value of  $L$  to provide a fair comparison: the errors plotted in Fig. 10 correspond to that morphological rule which results in minimum error for that value of  $L$ . (In addition to the alternatives shown in Table 1,  $n = 6, 7, 8$  thinning, and

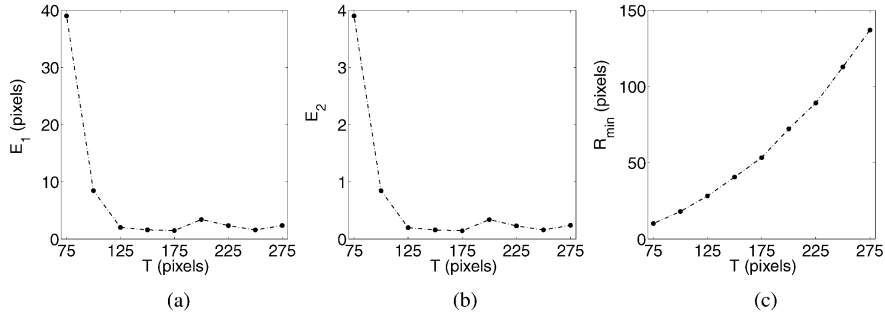


Fig. 7. (a)  $E_1$ , (b)  $E_2$ , (c)  $R_{min}$ , as the period of the sinusoid is varied.  $L = 200$  pixels,  $A = 30$  pixels, and the sensor beamwidth is  $30^\circ$ .

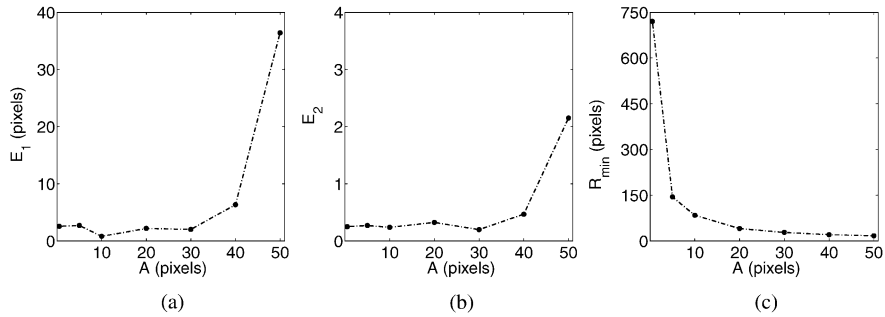


Fig. 8. (a)  $E_1$ , (b)  $E_2$ , (c)  $R_{min}$ , as the amplitude of the sinusoid is varied.  $T = 125$  pixels,  $L = 200$  pixels, and the sensor beamwidth is  $30^\circ$ .

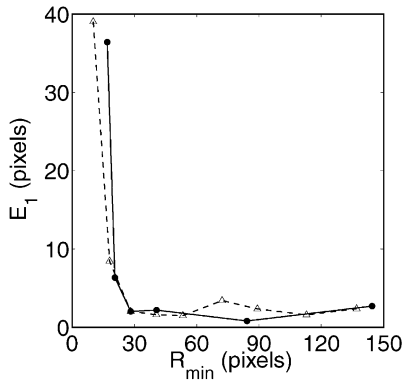


Fig. 9.  $E_1$  versus  $R_{min}$  when  $L = 200$  pixels. Solid dots connected by solid lines are produced by eliminating  $T$  from Figs. 7(a) and (c). Triangles connected by dashed lines are produced by eliminating  $A$  from Figs. 8(a) and (c).

also the application of no morphological processing at all have been considered.) For a given beamwidth, when the surface is located further, the arcs become larger and there is more uncertainty in the position of the reflection point(s). In a way, the “effective” curvature of the surface increases with increasing distance from the surface, resulting in larger errors. Geometrically, this is the same effect as perceiving a curved object to be flatter when we are very close to it, and more curved when further away. A distinct issue arises when the distances are very small:

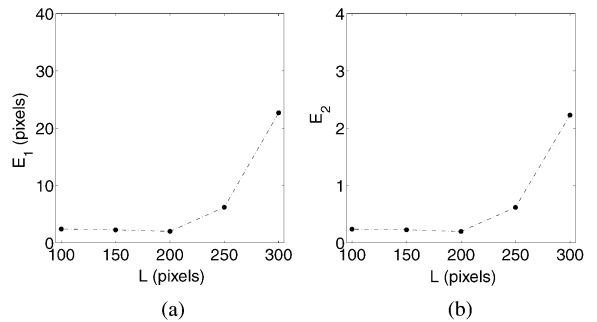


Fig. 10. (a)  $E_1$ , (b)  $E_2$ , as the surface distance is varied.  $T = 125$  pixels,  $A = 30$  pixels, and the sensor beamwidth is  $30^\circ$ .

the arcs become very small and less in number, since now sensors can detect a smaller portion of the surface and there is less overlap between their sensitivity patterns. As a result, the arc map cannot cover the whole surface.

### 3.4. The effect of varying the sensor beamwidth

Another important parameter is the sensor beamwidth. To investigate the effect of sensor beamwidth, the surface parameters are kept constant while the beamwidth is varied. Increasing the beamwidth results in arcs longer in length, causing a larger portion of each arc to be redundant. In other words, there is more uncertainty in

Table 2  
Variation of the errors with surface distance and the corresponding morphological operations

$L$ (pixels)	Morphological operation	$E_1$ (pixels)	$E_2$
100	Thinning ( $n = 1$ )	2.43	0.24
150	Thinning ( $n = 1$ )	2.29	0.23
200	Thinning ( $n = 3$ )	2.03	0.20
250	Thinning ( $n = 3$ )	6.22	0.63
300	Thinning ( $n = 4$ )	22.71	2.28

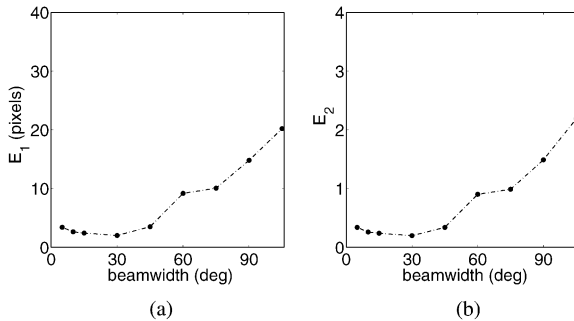


Fig. 11. (a)  $E_1$ , (b)  $E_2$ , as the beamwidth is varied.  $A = 30$  pixels,  $T = 125$  pixels, and  $L = 200$  pixels.

the position of the reflection point(s) as compared to the case of a narrower beamwidth. As a result, the errors tend to increase as shown in Fig. 11. The arcs also increase in number, and these factors make it necessary to apply higher  $n$  thinning to extract the useful information. On the other hand, when the beamwidth is very small, the arcs become very short and fewer in number, leading to a similar situation as when  $L$  was very small. The large number of simulations and experiments undertaken indicate that below a beamwidth of  $15^\circ$ , directly fitting a polynomial to whatever few points are available in the arc map, without applying morphological processing, becomes the best choice since the error in this case is smallest. This customization of the applied morphological rule enables a fair comparison of the results at all beamwidth values.

Smaller beamwidths result in fewer arc points and thus less reliable curve fits, leading to a slight increase in the error for very small beamwidths. Best results are obtained for a particular beamwidth (about  $30^\circ$  in our example). The different morphological operations applied and the resulting error values are tabulated in Table 3. Choosing beamwidths smaller than  $30^\circ$  does not increase the error appreciably, but using sensors with smaller beamwidths may not be desirable anyhow, since these are usually more difficult to manufacture, expensive, or entail a trade-off with some other quantity. For instance, in the case of acoustic sensors, narrower beam-

Table 3  
Simulation results for the data obtained from sensors with different beamwidth

Beamwidth (deg.)	Morphological operation	$E_1$ (pixels)	$E_2$
5	None	3.41	0.34
10	None	2.65	0.26
15	None	2.43	0.24
30	Thinning ( $n = 3$ )	2.03	0.20
45	Thinning ( $n = 5$ )	3.51	0.34
60	Thinning ( $n = 5$ )	9.19	0.90
75	Thinning ( $n = 6$ )	10.07	0.99
90	Thinning ( $n = 7$ )	14.82	1.49
105	Thinning ( $n = 8$ )	20.21	2.19

width devices must have higher operating frequencies, which in turn imply greater attenuation in air and thus shorter operating range.

### 3.5. The effect of the pixel size

Now, we discuss the issue of choice of sampling resolution or pixel size: There are a couple of factors that determine the accuracy of TOF readings in a range measurement system. One of these factors is the operating wavelength of the measurement system: a TOF measurement with accuracy better than the wavelength cannot be normally achieved. Other sources of uncertainty in the range measurement could be effects such as the thermal noise in the receiving circuitry or the ambient noise. Given these, it is not meaningful to choose the pixel size much smaller than the resolving limit determined by these factors since it would increase the computational burden without resulting in a more accurate profile determination. Thus, the pixel size should be chosen comparable to the TOF measurement accuracy. Nevertheless, since the TOF accuracy may not be known beforehand, in the following, we have also examined the cases where the noise or uncertainty is smaller, as well as larger than one pixel.

### 3.6. The effect of additive measurement noise

To investigate the robustness of the method to noise, zero-mean white Gaussian noise has been added to the TOF readings. As expected, for  $\sigma_n$  smaller than the order of one pixel, the performance is approximately the same as for the noiseless case. This performance can be further improved by reducing the pixel size until it becomes comparable to the TOF measurement accuracy, at the cost of greater computation time.

The error increases significantly as the noise level increases beyond 5–10 pixels (Fig. 13). Since the method relies on the mutual reinforcement of several arcs to

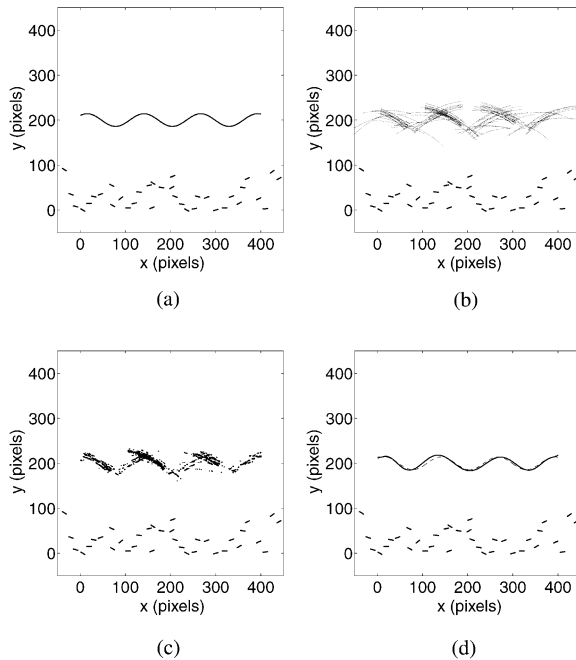


Fig. 12. (a) The actual surface, (b) the arc map obtained from noisy TOF measurements ( $\sigma_n = 5$  pixels), (c) the result of  $n = 3$  thinning, (d) the fitted curve (solid line) and the original surface (dashed line).  $E_1 = 3.28$  pixels,  $E_2 = 0.32$ .

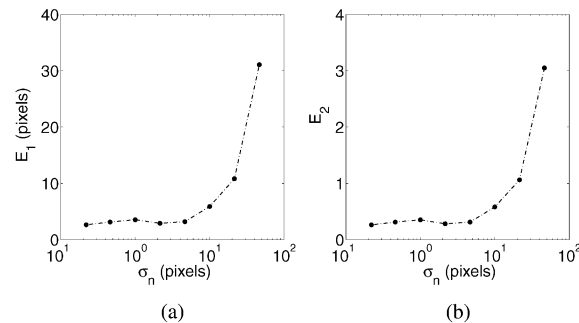


Fig. 13. (a)  $E_1$ , (b)  $E_2$ , as the standard deviation of the noise  $\sigma_n$  on the TOF readings is increased.  $A = 30$  pixels,  $T = 125$  pixels,  $L = 200$  pixels, and the sensor beamwidth is  $30^\circ$ .

reveal the surface, larger amounts of noise are expected to have a destructive effect on this process by moving the various arc segments out of their reinforcing positions. Consequently, the arc segments which now lack each other's mutual reinforcement tend to be eliminated by the morphological operations (Fig. 12). A larger proportion of the arcs is eliminated, resulting in a loss of information characterizing the original curve. Nevertheless, the error growth rate is not as high as might be suggested by these arguments, and the method seems to be reasonably robust to noise. In Fig. 13, the performance is comparable to the noiseless case up to  $\sigma_n = 10$

pixels. This is partly because the least-squares polynomial fit helps eliminate some of the noise.

#### 4. Conclusion

A novel method is described for determining arbitrary surface profiles by applying morphological processing to data acquired by simple range sensors. The method is extremely flexible, versatile, and robust, as well as being simple and straightforward. It can deal with arbitrary numbers and configurations of sensors, including synthetic arrays. Accuracy improves with the number of sensors used and can be as low as a few pixels. The method is robust in many aspects; it has the inherent ability to eliminate undesired TOF readings arising from higher-order reflections, crosstalk, and noise, as well as processing multiple echoes informatively.

The CPU times for the morphological operations (when implemented in the C programming language and run on a 200 MHz Pentium Pro PC) are generally about a quarter of a second [3], indicating that the method is viable for real-time applications. The method can be readily generalized to three-dimensional environments with the arcs replaced by spherical or elliptical caps and the morphological rules extended to three dimensions [18]. In certain problems, it may be preferable to reformulate the method in polar or spherical coordinates. Some applications may involve an inhomogeneous and/or anisotropic medium of propagation. It is envisioned that the method could be generalized in such cases by constructing broken or non-ellipsoidal arcs.

#### Acknowledgements

This work was supported by TÜBİTAK under grants 197E051, EEEAG-92, and EEEAG-116. The experiments were performed at Bilkent University Robotics and Sensing Laboratory. The authors would like to thank the anonymous reviewer for the useful comments and suggestions.

#### References

- [1] B. Barshan, R. Kuc, Differentiating sonar reflections from corners and planes by employing an intelligent sensor, *IEEE Trans. Pattern Anal. Mach. Intell.* 12 (6) (1990) 560–569.
- [2] M.K. Brown, The extraction of curved surface features with generic range sensors, *Int. J. Robotics Res.* 5 (1) (1986) 3–18.
- [3] D. Başkent, Surface profile determination from multiple sonar data using morphological processing, Master's Thesis, Bilkent University, Department of Electrical Engineering, Ankara, Turkey, July 1998.

- [4] E.R. Dougherty, An Introduction to Morphological Image Processing, SPIE Optical Engineering Press, Bellingham, WA, 1992.
- [5] A.N. Venetsanopoulos, P. Yu, V. Anastassopoulos, Pattern recognition based on morphological shape analysis and neural networks, *Math. Comput. Simulation* 40 (5–6) (1996) 577–595.
- [6] R. Brivot, J.A. Marchant, Segmentation of plants and weeds for a precision crop protection robot using infrared images, *IEE Proc. Vision Image Signal Process.* 143 (2) (1996) 118–124.
- [7] A. Mojsilovic, M. Popovic, N. Amodaj, R. Babic, M. Ostojic, Automatic segmentation of intravascular ultrasound images: a texture-based approach, *Ann. Biomed. Eng.* 25 (6) (1997) 1059–1071.
- [8] S. Krishnamurthy, S.S. Iyengar, R.J. Holyer, M. Lybanon, Histogram-based morphological edge detector, *IEEE Trans. Geosci. Remote Sensing* 32 (4) (1994) 759–767.
- [9] J. Cardillo, M.A. Sidahmed, Target recognition in a cluttered scene using mathematical morphology, *Pattern Recognition* 29 (1) (1996) 27–49.
- [10] J. Saniie, M.A. Mohamed, Ultrasonic flaw detection based on mathematical morphology, *IEEE Trans. Ultrasonics Ferroelectron. Frequency Control* 41 (1) (1994) 150–160.
- [11] D.L. Wilson, P. Dalal, K.S. Kump, W. Benard, P. Xue, R.E. Marchant, S.J. Eppell, Morphological modeling of atomic-force microscopy imaging including nanostructure probes and fibrinogen molecules, *J. Vacuum Sci. Technol. B* 14 (4) (1996) 2407–2416.
- [12] I. Pitas, A. Maglara, Range image analysis by using morphological signal decomposition, *Pattern Recognition* 24 (2) (1991) 165–181.
- [13] J.G. Verly, R.L. Delanoy, Some principles and applications of adaptive mathematical morphology for range imagery, *Opt. Eng.* 32 (12) (1993) 3295–3306.
- [14] I. Pitas, *Digital Image Processing Algorithms*, Prentice-Hall International, Hemel Hempstead, UK, 1993.
- [15] H.R. Myler, A.R. Weeks, *Computer Imaging Recipes in C*, Prentice-Hall, Englewood Cliffs, NJ, 1993.
- [16] D. Başkent, B. Barshan, Surface profile determination from multiple sonar data using morphological processing, *Int. J. Robotics Res.* 18 (8) (1999) 788–808.
- [17] B. Barshan, D. Başkent, Comparison of two methods of surface profile extraction from multiple ultrasonic range measurements, *Meas. Sci. Technol.* 11 (6) (2000) 833–844.
- [18] K. Preston, 3-dimensional mathematical morphology, *Image Vision Comput.* 9 (5) (1991) 285–295.

**About the Author**—BILLUR BARSHAN received B.S. degrees in both electrical engineering and in physics from Boğaziçi University, Istanbul, Turkey and the M.S. and Ph.D. degrees in electrical engineering from Yale University, New Haven, Connecticut, in 1986, 1988, and 1991, respectively. Dr. Barshan was a research assistant at Yale University from 1987 to 1991, a postdoctoral researcher at the Robotics Research Group at University of Oxford, U.K. from 1991 to 1993. She joined Bilkent University, Ankara in 1993 where she is currently associate professor at the Department of Electrical Engineering. Dr. Barshan has established the Robotics and Sensing Laboratory in the same department. She is the recipient of the 1994 Nakamura Prize awarded to the most outstanding paper in 1993 IEEE/RSJ Intelligent Robots and Systems International Conference, 1998 TÜBİTAK Young Investigator Award, and 1999 Mustafa N. Parlar Foundation Research Award. Dr. Barshan's current research interests include intelligent sensors, sonar and inertial navigation systems, sensor-based robotics, and multi-sensor data fusion.

**About the Author**—DENİZ BAŞKENT received the B.S. and M.S. degrees in electrical engineering from Bilkent University, Ankara, Turkey in 1996 and 1998, respectively, and is currently pursuing a Ph.D. degree at the Department of Biomedical Engineering at the University of Southern California, Los Angeles, California. Her current research interests include biomedical engineering, intelligent sensing, and sensor-based robotics.